


Thermal stability investigation for Ohmic contact properties of Pt, Au, and Pd electrodes on the same hydrogen-terminated diamond

Cite as: AIP Advances 10, 055114 (2020); <https://doi.org/10.1063/5.0008167>

Submitted: 23 March 2020 . Accepted: 02 May 2020 . Published Online: 13 May 2020

Xiaolu Yuan, Jiangwei Liu , Siwu Shao, Jinlong Liu , Junjun Wei, Bo Da , Chengming Li, and Yasuo Koide 



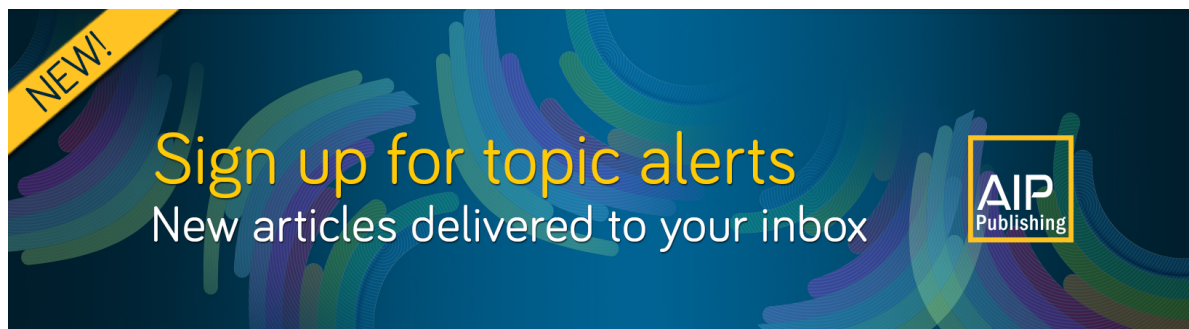
View Online



Export Citation



CrossMark



Thermal stability investigation for Ohmic contact properties of Pt, Au, and Pd electrodes on the same hydrogen-terminated diamond

Cite as: AIP Advances 10, 055114 (2020); doi: 10.1063/5.0008167

Submitted: 23 March 2020 • Accepted: 2 May 2020 •

Published Online: 13 May 2020



Xiaolu Yuan,^{1,2} Jiangwei Liu,^{2,a)} Siwu Shao,¹ Jinlong Liu,¹ Junjun Wei,¹ Bo Da,³ Chengming Li,^{1,a)} and Yasuo Koide²

AFFILIATIONS

¹Institute for Advanced Materials and Technology, University of Science and Technology Beijing, Beijing 100083, China

²Research Center for Functional Materials, National Institute for Materials Science (NIMS), 1-1 Namiki, Tsukuba, Ibaraki 305-0044, Japan

³Research and Services Division of Materials Data and Integrated System, NIMS, 1-1 Namiki, Tsukuba, Ibaraki 305-0044, Japan

^{a)}Authors to whom correspondence should be addressed: Liu.jiangwei@nims.go.jp and Chengmli@mater.ustb.edu.cn

ABSTRACT

Here, thermal stabilities for Ohmic contact properties of Pt, Au, and Pd on the same hydrogen-terminated diamond (H-diamond) epitaxial layer are investigated. A long-term annealing process is performed with an annealing temperature and time of 400 °C and 8 h, respectively. Before annealing, good Ohmic contact properties are observed for only two contacts of the Pt/H-diamond and Pd/H-diamond with specific contact resistivity (ρ_C) values of $2.7 \times 10^{-3} \Omega \text{ cm}^2$ and $2.6 \times 10^{-4} \Omega \text{ cm}^2$, respectively. After long-term annealing, all three contacts on the H-diamond show good Ohmic contact properties. The ρ_C values for the Pt/H-diamond and Au/H-diamond are $3.1 \times 10^{-2} \Omega \text{ cm}^2$ and $4.2 \times 10^{-4} \Omega \text{ cm}^2$, respectively. They are higher than that of the Pd/H-diamond ($1.1 \times 10^{-4} \Omega \text{ cm}^2$). Therefore, low ρ_C and good thermal stability for the Pd/H-diamond are achieved. This is meaningful for pushing forward the development of H-diamond-based electronic devices for high-temperature applications.

© 2020 Author(s). All article content, except where otherwise noted, is licensed under a Creative Commons Attribution (CC BY) license (<http://creativecommons.org/licenses/by/4.0/>). <https://doi.org/10.1063/5.0008167>

Semiconductor diamonds have many remarkable intrinsic properties, such as wide bandgap energy (5.47 eV), highest thermal conductivity (22 W/cm K), high carrier mobilities (4500 cm²/V s and 3800 cm²/V s for electrons and holes, respectively), and high breakdown electric field (10 MV/cm).^{1–4} Therefore, diamond appears promising for producing next-generation high-power, high-frequency, and high-temperature electronic devices.^{5–7} Currently, the hydrogen-terminated diamond (H-diamond) and bulk-doped diamond (such as boron-doped and phosphorous-doped) are used for the fabrication of metal-oxide-semiconductor field-effect transistors (MOSFETs).^{8–13} However, current outputs of bulk-doped diamond-based MOSFETs are quite low (<1.6 mA/mm) due to the high activation energies of dopants.^{8,9} In contrast, H-diamond-based MOSFETs have much higher current densities, thanks to their good surface conductivity with a sheet hole density of

$\sim 10^{14}/\text{cm}^2$.¹⁰ The current output maximum for H-diamond-based MOSFETs was as high as 1350 mA/mm.¹⁰ Furthermore, they could operate well with a cutoff frequency and breakdown voltage of 70 GHz and 2000 V, respectively.^{11,12} These electrical properties make H-diamond-based MOSFETs promising for high-power and high-frequency applications.

For H-diamond-based MOSFETs, another important consideration is high-temperature applications. Recently, it was reported that H-diamond-based MOSFETs could work well at temperatures as high as 400 °C.¹³ In order to further improve the performance of H-diamond-based MOSFETs at high-temperature, it is important to find a suitable metal electrode on the H-diamond to form Ohmic contacts with a low specific contact resistivity (ρ_C) and good thermal stability. In order to obtain Ohmic contacts on the *p*-type H-diamond, a metal electrode with a work function (Φ_M) larger than

that of the H-diamond (Φ_M : 4.9 eV) is required.¹⁴ Until now, several metals such as Au (Φ_M : 5.10 eV), Pt (Φ_M : 5.65 eV), Pd (Φ_M : 5.12 eV), and 500 °C-annealed Ti/Au (Φ_M : 4.33/5.10 eV) have been used as Ohmic contacts on the H-diamond.^{15–20} However, their thermal stability has been rarely reported. On the other hand, Ohmic contacts on the H-diamond are affected by the quality of the H-diamond epitaxial layer, which depends on the growth conditions. The contact properties of metal electrodes on different H-diamond epitaxial layers are therefore difficult to be compared with each other.

In this study, Pt, Au, and Pd electrodes are formed on the same H-diamond epitaxial layer. Their specific contact resistivities and thermal stabilities at the maximum operation temperature (400 °C) of H-diamond MOSFETs will be investigated and discussed.

Three electrodes were formed separately on the H-diamond. Figure 1 shows the formation routines of the Pt contact on the H-diamond epitaxial layer. The Ib-type single-crystalline diamond (100) substrate with dimensions of $3.0 \times 3.0 \times 1.0 \text{ mm}^3$ was cleaned in a mixed acid (H_2SO_4 and HNO_3 with a volume ratio of 1:1) at 300 °C for 3 h [Fig. 1(a)]. The H-diamond was homoepitaxially grown with a thickness of 150 nm using a microwave plasma-enhanced chemical vapor deposition system (No. AX5200S, Seki Technotron Corp., Tokyo, Japan) [Fig. 1(b)]. The CH_4 flow rate, H_2 flow rate, chamber pressure, growth temperature, and growth time were 0.5 SCCM, 500 SCCM, 80 Torr, 900–940 °C, and 1.5 h, respectively. Surface roughness of the H-diamond epitaxial layer was previously reported to be around 1.2 nm via an atomic force microscopy technique.²¹ Its sheet hole density and mobility were confirmed to be around $\sim 10^{13}/\text{cm}^2$ and $90 \text{ cm}^2/\text{V s}$, respectively, using the Hall measurement system. For each following step of the key-pattern formation [Fig. 1(c)], mesa-structure formation [Fig. 1(d)], contact electrode formation [Fig. 1(e)], and coating, exposing, developing, and lifting-off of photoresists were performed. The sample was sequentially coated with LOR5A and AZ5214E positive photoresists using a spin-coater with a rotation rate and time of 7000 rpm and 1 s, respectively. The baking temperature and time for the LOR5A/AZ5214E photoresists were 180/110 °C and 5/2 min, respectively. After being exposed to a mask-less photolithography system (No. DL-1000/NC2P, Nanosystem Solutions, Inc. Tokyo,

Japan) with a dose energy of $250 \text{ mJ}/\text{cm}^2$, the sample was developed in a 2.38% tetramethyl ammonium hydroxide (TMAH) solution for 90 s.

Cross-shaped key-patterns [Fig. 1(c)] were formed using a *J*-sputter system (No. CFS-4EP-LL, Shibaura Mechatronics Corp., Kanagawa, Japan) at an Ar atmosphere for calibrating the positions of the mesa-structure [Fig. 1(d)] and Ohmic contacts [Fig. 1(e)]. The mesa-structure for the H-diamond was formed using a capacitively coupled-plasma reactive ion etching system (No. RIE-200NL, Samco Inc., Kyodo, Japan) [Fig. 1(d)]. The plasma power, O_2 flow rate, and etching time were 50 W, 100 SCCM, and 90 s, respectively. The Pt metal covered by the Ti/Au bilayer on the H-diamond was formed via an e-beam evaporation system (No. RDEB-1206K, R-DEC. Co., Ltd., Ibaraki, Japan) under a vacuum condition of $\sim 10^{-5} \text{ Pa}$ [Fig. 1(e)]. After lifting-off of the photoresists in an *n*-methylpyrrolidone (NMP) solution for 3 h at room temperature, the Au and Pd (covered by the Ti/Au) electrodes were formed with the same evaporation system separately. The Ti/Au cover layers are important to prevent oxidation of Pt and Pd in air. Thicknesses of the Pt/Ti/Au, Au, and Pd/Ti/Au metals were 10/20/100, 100, and 10/20/100 nm, respectively. After finishing the formation process, the sample was annealed at 400 °C for as long as 8 h under a low vacuum condition ($\sim 5.0 \text{ Pa}$) via a rapid thermal annealing system (No. QHC-P410, Advance Riko, Inc., Kanagawa, Japan). Then, the sample was exposed to atmosphere for more than 24 h to saturate the conductivity of the H-diamond surface.²² Electrical properties of the three contacts on the H-diamond were characterized using a four-probe system (Vector Semiconductor Co., Ltd., Tokyo, Japan) at room temperature.

Figure 2(a) shows the surface morphology of the three contacts on the H-diamond. The length and width for each electrode are the same, $100 \mu\text{m}$. No electrodes peeled-off after the formation process. There are eight different interspace (d) values between two adjacent electrodes for each contact. Interspace distances between them are confirmed via a scanning electron microscope technique after electrical property measurement [Fig. 2(b)]. The d values are in the range of $5.0 \mu\text{m}$ – $18.5 \mu\text{m}$, $4.8 \mu\text{m}$ – $18.8 \mu\text{m}$, and $4.9 \mu\text{m}$ – $19.0 \mu\text{m}$ for the Pt, Au, and Pd contacts, respectively.

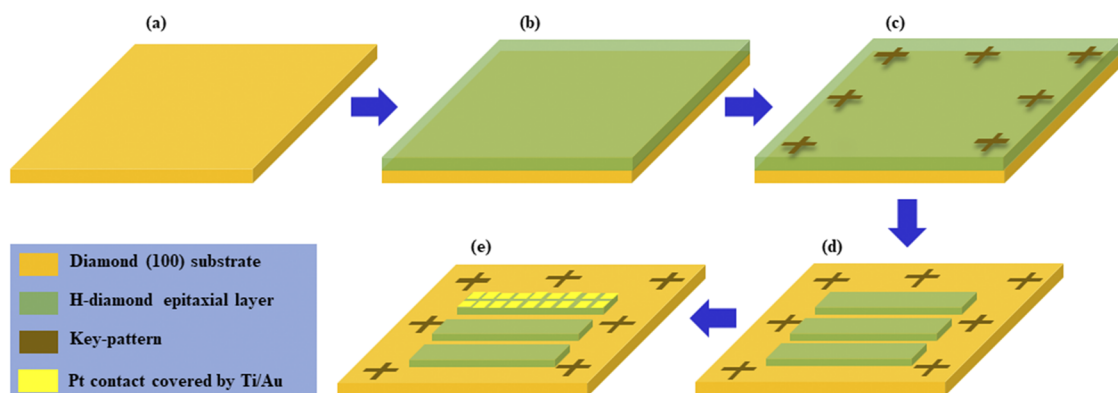


FIG. 1. Formation routines of the Pt contact on the H-diamond epitaxial layer: (a) the diamond (100) substrate, (b) H-diamond epitaxial layer growth, (c) key-pattern formation, (d) mesa-structure formation, and (e) the Pt contact covered by Ti/Au.

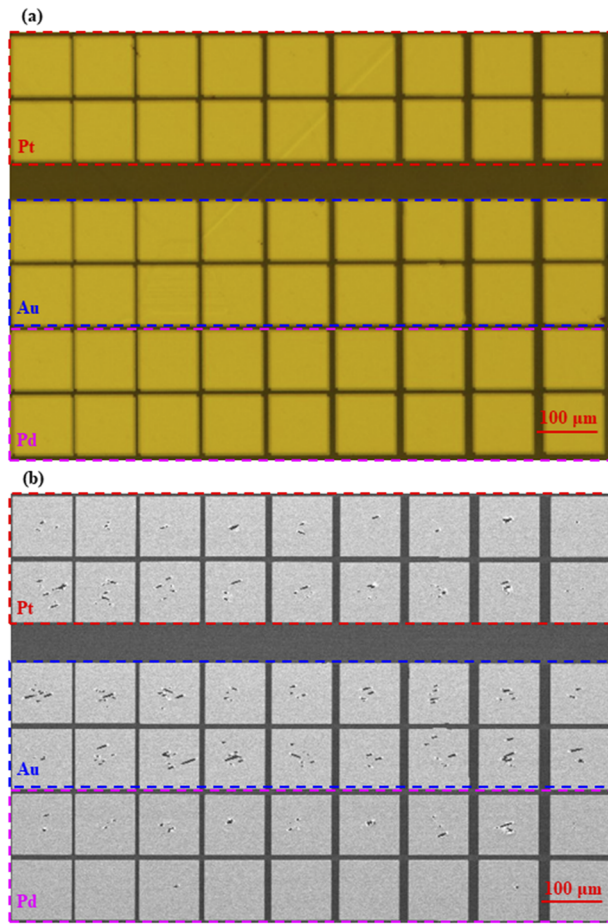


FIG. 2. (a) Surface morphologies of three contacts on the H-diamond before annealing and (b) its scanning electron microscope images after annealing and electrical property measurement.

Figures 3(a) and 3(c) show the current–voltage characteristics of the Pt/H-diamond before and after annealing at 400 °C for 8 h, respectively. The voltage was changed from -0.5 V to 0.5 V. The current was normalized by an electrode width of $100\ \mu\text{m}$. All current–voltage curves have linear characteristics, implying good Ohmic contact properties for the Pt/H-diamond before and after annealing. When d is $5.0\ \mu\text{m}$, the current is 6.7×10^{-4} A/mm at a voltage of 0.5 V before annealing, which is higher than that (1.7×10^{-4} A/mm) after annealing. Total resistance (R_T) values for the Pt/H-diamond at $d = 5.0\ \mu\text{m}$ before and after annealing are calculated to be $7.5 \times 10^2\ \Omega\ \text{mm}$ and $2.9 \times 10^3\ \Omega\ \text{mm}$, respectively. The increase in R_T after annealing is possibly due to the deterioration of surface conductivity of the H-diamond.²² Figures 3(b) and 3(d) show R_T as functions of d for the Pt/H-diamond before and after annealing, respectively. The black triangle and red square spots represent R_T at voltages of -0.5 V and 0.5 V, respectively. With the change in d from $5.0\ \mu\text{m}$ to $18.5\ \mu\text{m}$, R_T increases. R_T between two adjacent Ohmic electrodes is twice the contact resistance (R_C) and surface

resistance (R_S), as shown in the following equation:^{23,24}

$$R_T = 2R_C + R_S, \quad (1)$$

$$R_S = R_{\text{sheet}} \times d, \quad (2)$$

where R_{sheet} is the surface sheet resistance. If $2R_C$ for the two adjacent Ohmic electrodes are stable, the increase in R_T with a change in d is attributed to R_S . By fitting the spots in Figs. 3(b) and 3(d), the $2R_C$ values (the intercepts of the y -axis for the fitting lines) for the Pt/H-diamond before and after annealing are determined to be $3.5 \times 10^2\ \Omega\ \text{mm}$ and $1.9 \times 10^3\ \Omega\ \text{mm}$, respectively. Their R_{sheet} values extracted from the slopes of the fitting lines are determined to be $1.1 \times 10^5\ \Omega/\square$ and $2.9 \times 10^5\ \Omega/\square$, respectively. Therefore, R_{sheet} for the H-diamond increases after long-term annealing, which can be ascribed to the damage of the surface adsorbates and C–H bonds on the H-diamond.²² Their twice the transfer length ($2L_T$) (the intercept of the x -axis for the fitting lines) is calculated to be $3.1\ \mu\text{m}$ and $6.6\ \mu\text{m}$, respectively. Therefore, the ρ_C values for the Pt/H-diamond before and after annealing are calculated to be $2.7 \times 10^{-3}\ \Omega\ \text{cm}^2$ and $3.1 \times 10^{-2}\ \Omega\ \text{cm}^2$, respectively, based on the following equation:^{23,24}

$$\rho_C = R_C \cdot L_T. \quad (3)$$

Figures 4(a) and 4(b) show the current–voltage characteristics of the Au/H-diamond before and after annealing, respectively. Before annealing, there were not good linear relationships for all the curves. Meanwhile, the current at a voltage of 0.5 V is disordered with the increase in d from $4.8\ \mu\text{m}$ to $18.8\ \mu\text{m}$. The poor Ohmic contact properties for the Au/H-diamond before annealing are possibly attributed to the adhesion issue of Au on the H-diamond.²⁵ After annealing at 400 °C for 8 h, there are good linear relationships for the current–voltage curves, as shown in Fig. 4(c). The current at $d = 4.8\ \mu\text{m}$ is 4.2×10^{-4} A/mm, which is one order larger than that before annealing. Figures 4(b) and 4(d) show R_T as functions of d for the Au/H-diamond before and after annealing, respectively. Before annealing, the black triangle (the R_T calculated at -0.5 V) and red square (the R_T calculated at 0.5 V) spots are quite different from each other at the same d value. It is difficult to deduce the $2R_C$ and $2L_T$ values. After annealing, the black triangle and red square spots are in good agreement with each other. Therefore, $2R_C$, R_{sheet} , and $2L_T$ for the Au/H-diamond after annealing are calculated to be $2.1 \times 10^2\ \Omega\ \text{mm}$, $2.7 \times 10^5\ \Omega/\square$, and $0.8\ \mu\text{m}$, respectively. Its ρ_C can be calculated, based on Eq. (2), to be $4.2 \times 10^{-4}\ \Omega\ \text{cm}^2$, which is lower than those of the Pt/H-diamond before ($2.7 \times 10^{-3}\ \Omega\ \text{cm}^2$) and after annealing ($3.1 \times 10^{-2}\ \Omega\ \text{cm}^2$). However, it is larger than that of the 600 °C-annealed Au/H-diamond ($4.3 \times 10^{-5}\ \Omega\ \text{cm}^2$).²⁶ Therefore, a higher annealing temperature for the Au/H-diamond contact would further decrease its ρ_C .

Figures 5(a) and 5(c) show the current–voltage characteristics of the Pd/H-diamond before and after annealing, respectively. For all current–voltage curves, there are linear characteristics. Good Ohmic contacts for the Pd/H-diamond are obtained. Before annealing, the current at a voltage of 0.5 V is 1.2×10^{-3} A/mm at $d = 4.9\ \mu\text{m}$. After annealing, it decreases to 3.6×10^{-4} A/mm. R_T as functions of d for the Pd/H-diamond before and after annealing are shown in Figs. 5(b) and 5(d), respectively. The black triangle (the R_T calculated at -0.5 V) and red square (the R_T calculated at 0.5 V) spots are in good agreement with each other. By fitting them, $2R_C$ for the Pd/H-diamond before and after annealing is determined

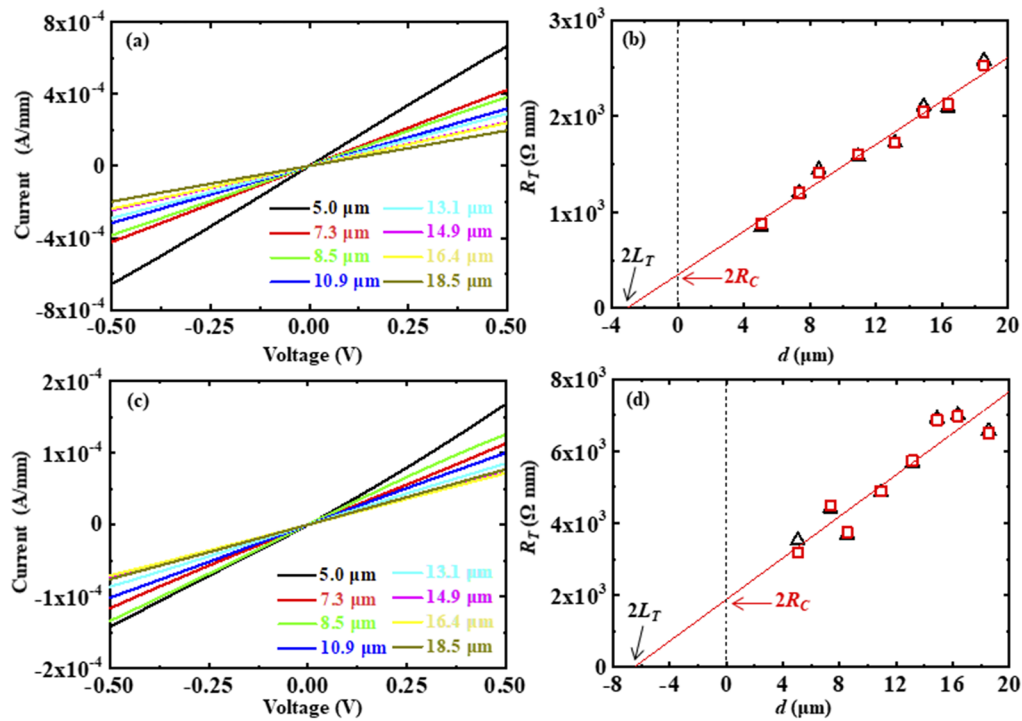


FIG. 3. (a) and (c) Current–voltage characteristics of the Pt/H-diamond before annealing and after annealing, respectively and (b) and (d) R_T as functions of d before and after annealing, respectively. Black triangle and red square spots represent the R_T values calculated at voltages of -0.5 V and 0.5 V , respectively.

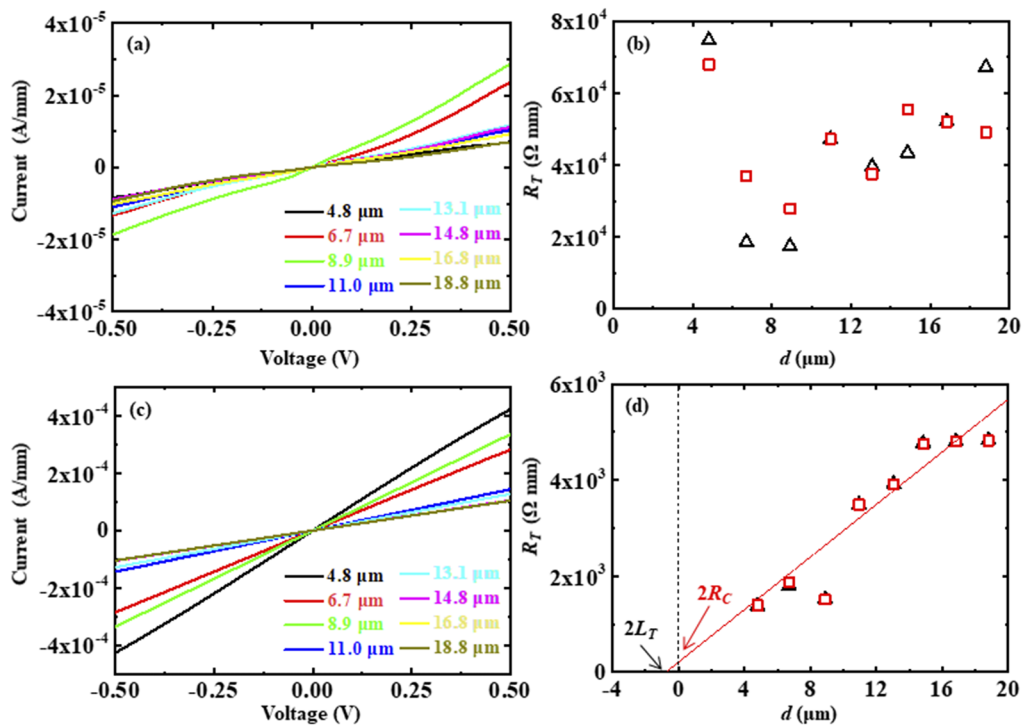


FIG. 4. (a) and (c) Current–voltage characteristics of the Au/H-diamond before annealing and after annealing, respectively and (b) and (d) R_T as functions of d before and after annealing, respectively. Black triangle and red square spots represent the R_T values calculated at voltages of -0.5 V and 0.5 V , respectively.

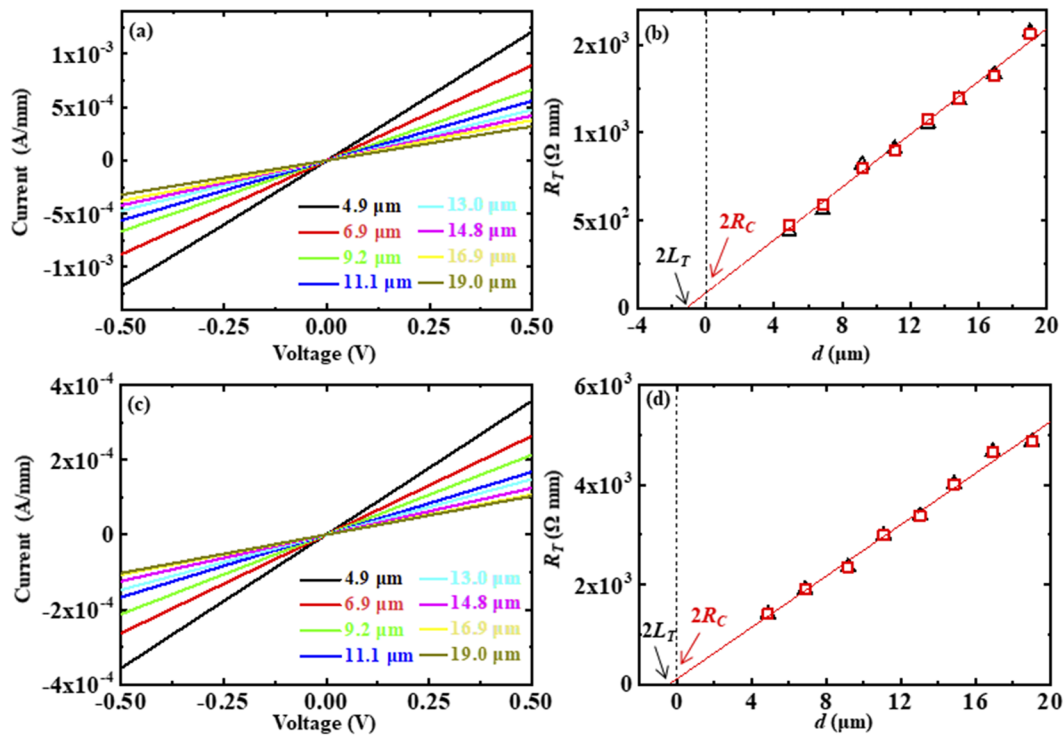


FIG. 5. (a) and (c) Current–voltage characteristics of the Pd/H-diamond before annealing and after annealing, respectively and (b) and (d) R_T as functions of d before and after annealing, respectively. Black triangle and red square spots represent the R_T values calculated at voltages of -0.5 V and 0.5 V, respectively.

to be $86.7 \Omega \text{ mm}$ and $110.0 \Omega \text{ mm}$, respectively. R_{sheet} for the H-diamond surfaces is $7.5 \times 10^4 \Omega/\square$ and $2.6 \times 10^5 \Omega/\square$, respectively. The $2L_T$ values are deduced to be $1.2 \mu\text{m}$ and $0.4 \mu\text{m}$, respectively. The ρ_C values for the Pd/H-diamond before and after annealing are calculated, based on Eq. (3), to be $2.6 \times 10^{-4} \Omega \text{ cm}^2$ and $1.1 \times 10^{-4} \Omega \text{ cm}^2$, respectively, which are lower than that of the recently reported value ($8 \pm 1 \times 10^{-4} \Omega \text{ cm}^2$) for the Pd/H-diamond at room temperature.²⁰

Figures 6(a) and 6(b) summarize the annealing effects on R_C and ρ_C for three contacts on the H-diamond, respectively. Because

of the poor Ohmic contact for the Au/H-diamond before annealing, its R_C and ρ_C are not obtained. Annealing makes the R_C increase to more than five times that before annealing for the Pt/H-diamond. However, annealing does not affect R_C of the Pd/H-diamond greatly. Before annealing, R_C for the Pd/H-diamond is lower than that for the Pt/H-diamond. After annealing, it is still much lower than those of the Pt/H-diamond and Au/H-diamond. Annealing makes ρ_C for the Pt/H-diamond increase by around one order of magnitude compared with that before annealing [Fig. 6(b)]. It is also much larger than those of the Au/H-diamond and Pd/H-diamond. The ρ_C for

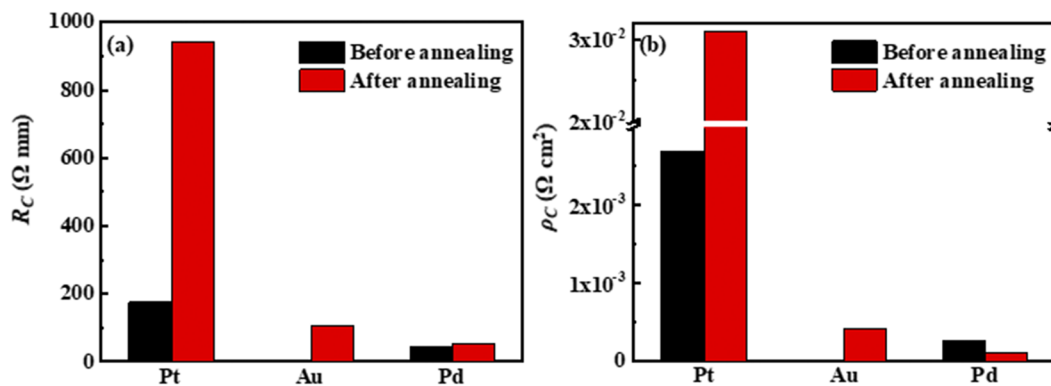


FIG. 6. Summary of (a) R_C and (b) ρ_C of three contacts on the H-diamond before and after annealing.

the Pd/H-diamond after annealing is a little lower than that before annealing and is also the lowest one among the three contacts. Based on the above comparisons for the three contacts shown in Figs. 6(a) and 6(b), it can be concluded that annealing degrades and improves the contact properties of the Pt/H-diamond and Au/H-diamond, respectively. After the long-term annealing process, the contact properties of the Pd/H-diamond are still very good and stable. Therefore, Pd is a good choice as an Ohmic contact electrode to push forward the development of H-diamond-based electronic devices for high-temperature applications.

In conclusion, the contact properties and thermal stabilities of Pt, Au, and Pd contacts on the same H-diamond epitaxial layer were investigated and discussed. Before annealing, only the Pt/H-diamond and Pd/H-diamond showed good Ohmic contact properties, with a ρ_C of $2.7 \times 10^{-3} \Omega \text{ cm}^2$ and $2.6 \times 10^{-4} \Omega \text{ cm}^2$, respectively. After annealing at 400°C for as long as 8 h, a good Ohmic contact was observed for all three contacts, with a ρ_C values of $3.1 \times 10^{-2} \Omega \text{ cm}^2$, $4.2 \times 10^{-4} \Omega \text{ cm}^2$, and $1.1 \times 10^{-4} \Omega \text{ cm}^2$, respectively. The long-term annealing process degrades and improves the contact properties of the Pt/H-diamond and Au/H-diamond, respectively. They were still stable for the Pd/H-diamond and were better than those of the other two contacts.

This work was supported by the KAKENHI Project, under Grant Nos. JP18K13806 and JP16H06419, the Leading Initiative for Excellent Young Researchers Program Project, the NIMS Nanofabrication Platform of the Nanotechnology Platform Project sponsored by the Ministry of Education, Culture, Sports, and Technology, Japan, and the Murata Science Foundation. It was supported partly by the National Key Research and Development Program of China (Grant No. 2016YFE0133200).

DATA AVAILABILITY

The data that support the findings of this study are available from the corresponding author upon reasonable request.

REFERENCES

- ¹C. J. H. Wort and R. S. Balmer, *Mater. Today* **11**, 22 (2008).
- ²J. Isberg, J. Hammersberg, E. Johansson, T. Wikström, D. J. Twitchen, A. J. Whitehead, S. E. Coe, and G. A. Scarsbrook, *Science* **297**, 1670 (2002).
- ³M. C. Rossi, S. Salvatori, and F. Galluzzi, *J. Vac. Sci. Technol., B* **16**, 1725 (1998).
- ⁴L. Reggiani, S. Bosi, C. Canali, F. Nava, and S. F. Kozlov, *Phys. Rev. B* **23**, 3050 (1981).
- ⁵H. Umezawa, M. Nagase, Y. Kato, and S.-i. Shikata, *Diamond Relat. Mater.* **24**, 201 (2012).
- ⁶S. Russell, S. Sharabi, A. Tallaie, and D. A. J. Moran, *IEEE Trans. Electron Devices* **62**, 751 (2015).
- ⁷S. Shikata, *Diamond Relat. Mater.* **65**, 168 (2016).
- ⁸T.-T. Pham, J. Pernot, G. Perez, D. Eon, E. Gheeraert, and N. Rouger, *IEEE Electron Device Lett.* **38**, 1571 (2017).
- ⁹T. Matsumoto, H. Kato, K. Oyama, T. Makino, M. Ogura, D. Takeuchi, T. Inokuma, N. Tokuda, and S. Yamasaki, *Sci. Rep.* **6**, 31585 (2016).
- ¹⁰K. Hiram, H. Sato, Y. Harada, H. Yamamoto, and M. Kasu, *Jpn. J. Appl. Phys., Part 1* **51**, 090112 (2012).
- ¹¹X. Yu, J. Zhou, C. Qi, Z. Cao, Y. Kong, and T. Chen, *IEEE Electron Device Lett.* **39**, 1373 (2018).
- ¹²Y. Kitabayashi, T. Kudo, H. Tsuboi, T. Yamada, D. Xu, M. Shibata, D. Matsumura, Y. Hayashi, M. Syamsul, M. Inaba, A. Hiraiwa, and H. Kwarada, *IEEE Electron Device Lett.* **38**, 363 (2017).
- ¹³H. Kwarada, H. Tsuboi, T. Naruo, T. Yamada, D. Xu, A. Daicho, T. Saito, and A. Hiraiwa, *Appl. Phys. Lett.* **105**, 013510 (2014).
- ¹⁴B. Rezek, C. Sauerer, C. E. Nebel, M. Stutzmann, J. Ristein, L. Ley, E. Snidero, and P. Bergonzo, *Appl. Phys. Lett.* **82**, 2266 (2003).
- ¹⁵H. B. Michaelson, *J. Appl. Phys.* **48**, 4729 (1977).
- ¹⁶Z. Ren, J. Zhang, J. Zhang, C. Zhang, S. Xu, Y. Li, and Y. Hao, *IEEE Electron Device Lett.* **38**, 786 (2017).
- ¹⁷M. Zhang, F. Lin, W. Wang, F. Li, Y.-F. Wang, H. Abbasi, D. Zhao, G. Chen, F. Wen, J. Zhang, R. Bu, and H. Wang, *Coatings* **9**, 539 (2019).
- ¹⁸J. W. Liu, H. Oosato, M. Y. Liao, M. Imura, E. Watanabe, and Y. Koide, *Appl. Phys. Lett.* **112**, 153501 (2018).
- ¹⁹M. Inaba, T. Muta, M. Kobayashi, T. Soito, M. Shibata, D. Matsumura, T. Kudo, A. Hiraiwa, and H. Kwarada, *Appl. Phys. Lett.* **109**, 033503 (2016).
- ²⁰K. Xing, A. Tsai, S. Rubanov, D. L. Creedon, S. A. Yianni, L. Zhang, W.-C. Hao, J. Zhuang, J. C. McCallum, C. I. Pakes, and D.-C. Qi, *Appl. Phys. Lett.* **116**, 111601 (2020).
- ²¹R. G. Banal, M. Imura, J. Liu, and Y. Koide, *J. Appl. Phys.* **120**, 115307 (2016).
- ²²F. Maier, M. Riedel, B. Mantel, J. Ristein, and L. Ley, *Phys. Rev. Lett.* **85**, 3472 (2000).
- ²³H. H. Berger, *Solid-State Electron.* **15**, 145 (1972).
- ²⁴D. K. Schroder, *Semiconductor Material and Device Characterization*, 3rd ed. (John Wiley & Sons, Inc., New York, 1998).
- ²⁵W. Wang, C. Hu, F. N. Li, S. Y. Li, Z. C. Liu, F. Wang, J. Fu, and H. X. Wang, *Diamond Relat. Mater.* **59**, 90 (2015).
- ²⁶J.-I. Liu, C.-m. Li, R.-h. Zhu, L.-x. Chen, J.-j. Wang, and Z.-h. Feng, *Int. J. Miner., Metall. Mater.* **20**, 802 (2013).